Locating the inner edge of the neutron star crust using terrestrial nuclear laboratory data

Jun Xu,[1] Lie-Wen Chen,[1,2] Bao-An Li,[3] and Hong-Ru Ma[1]

[1]*Institute of Theoretical Physics, Shanghai Jiao Tong University, Shanghai 200240, People's Republic of China*
[2]*Center of Theoretical Nuclear Physics, National Laboratory of Heavy-Ion Accelerator, Lanzhou 730000, People's Republic of China*
[3]*Department of Physics, Texas A&M University-Commerce, Commerce, Texas 75429-3011, USA*

Within both dynamical and thermodynamical approaches using the equation of state for neutron-rich nuclear matter constrained by the recent isospin diffusion data from heavy-ion reactions in the same subsaturation density range as the neutron star crust, the density and pressure at the inner edge separating the liquid core from the solid crust of neutron stars are determined to be 0.040 fm$^{-3} \leqslant \rho_t \leqslant$ 0.065 fm^{-3} and 0.01 MeV/fm$^3 \leqslant P_t \leqslant$ 0.26 MeV/fm^3, respectively. These together with the observed minimum crustal fraction of the total moment of inertia allow us to set a new limit for the radius of the Vela pulsar significantly different from the previous estimate. It is further shown that the widely used parabolic approximation to the equation of state of asymmetric nuclear matter leads systematically to significantly higher core-crust transition densities and pressures, especially with stiffer symmetry energy functionals.

I. INTRODUCTION

Having been the major testing grounds of our knowledge on the nature of matter under extreme conditions, neutron stars are among the most mysterious objects in the universe. To understand their structures and properties has long been a very challenging task for both the astrophysics and the nuclear physics community [1]. Theoretically, neutron stars are expected to have a solid inner crust surrounding a liquid core. Knowledge on properties of the crust plays an important role in understanding many astrophysical observations [2–12]. The inner crust spans the region from the neutron drip-out point to the inner edge separating the solid crust from the homogeneous liquid core. While the neutron drip-out density $\rho_{\rm out}$ is relatively well determined to be about 4×10^{11} g/cm^3 [13], the transition density ρ_t at the inner edge is still largely uncertain mainly because of our very limited knowledge on the equation of state (EOS), especially the density dependence of the symmetry energy, of neutron-rich nucleonic matter [6,7]. These uncertainties have hampered our accurate understanding of many important properties of neutron stars [1,6,7].

Recently, significant progress has been made in constraining the EOS of neutron-rich nuclear matter using terrestrial laboratory experiments (See Ref. [14] for the most recent review). In particular, the analysis of isospin-diffusion data [15–17] in heavy-ion collisions has constrained tightly the density dependence of the symmetry energy in exactly the same subsaturation density region around the expected inner edge of neutron star crusts. Moreover, the obtained constraint on the symmetry energy was found to agree with isoscaling analyses in heavy-ion collisions [18], the isotopic dependence of the giant monopole resonance in even-*A* Sn isotopes [19], and the neutron-skin thickness of ^{208}Pb [17,20,21]. In this article, using the equation of state for neutron-rich nuclear matter constrained by the recent isospin diffusion data from heavy-ion reactions in the same subsaturation density range as the neutron star crust, we determine the inner edge of neutron star crusts. Consequently, the limit on the radius of

the Vela pulsar is significantly different from the previous estimate. In addition, we find that the widely used parabolic approximation (PA) to the EOS of asymmetric nuclear matter enhances significantly the transition densities and pressures, especially with stiffer symmetry energy functionals.

II. THE THEORETICAL METHOD

The inner edge corresponds to the phase transition from the homogeneous matter at high densities to the inhomogeneous matter at low densities. In principle, the inner edge can be located by comparing in detail relevant properties of the nonuniform solid crust and the uniform liquid core mainly consisting of neutrons, protons, and electrons (*npe* matter). However, this is practically very difficult because the inner crust may contain nuclei having very complicated geometries, usually known as the "nuclear pasta" [1,10,22–24]. Furthermore, the core-crust transition is thought to be a very weak first-order phase transition and model calculations lead to very small density discontinuities at the transition [5,25–27]. In practice, therefore, a good approximation is to search for the density at which the uniform liquid first becomes unstable against small amplitude density fluctuations with clusterization. This approximation has been shown to produce a very small error for the actual core-crust transition density and it would yield the exact transition density for a second-order phase transition [5,25–27]. Several such methods including the dynamical method [2–5,25,28,29], the thermodynamical method [7,30,31], and the random phase approximation (RPA) [27,32] have been applied extensively in the literature. Here, we use both the dynamical and the thermodynamical methods.

In the dynamical method, the stability condition of a homogeneous *npe* matter against small periodic density perturbations with clusterization can be well approximated by [2–5,28]

$$V_{\rm dyn}(k) = V_0 + \beta k^2 + \frac{4\pi e^2}{k^2 + k_{TF}^2} > 0, \qquad (1)$$

where

$$V_0 = \frac{\partial \mu_p}{\partial \rho_p} - \frac{(\partial \mu_n / \partial \rho_p)^2}{\partial \mu_n / \partial \rho_n}, \quad k_{TF}^2 = \frac{4\pi e^2}{\partial \mu_e / \partial \rho_e},$$

$$\beta = D_{pp} + 2D_{np}\zeta + D_{nn}\zeta^2, \quad \zeta = -\frac{\partial \mu_n / \partial \rho_p}{\partial \mu_n / \partial \rho_n},$$

and k is the wave vector of the spatially periodic density perturbations and μ_i is the chemical potential of particle i. In the above expressions, we used the relation $\frac{\partial \mu_n}{\partial \rho_p} = \frac{\partial \mu_p}{\partial \rho_n}$ following $\frac{\partial \mu_n}{\partial \rho_p} = \frac{\partial}{\partial \rho_p}(\frac{\partial \varepsilon}{\partial \rho_n}) = \frac{\partial}{\partial \rho_n}(\frac{\partial \varepsilon}{\partial \rho_p}) = \frac{\partial \mu_p}{\partial \rho_n}$, with ε being the energy density of the *npe* matter. The three terms in Eq. (1) represent, respectively, the contributions from the bulk nuclear matter, the density gradient (surface) terms, and the Coulomb interaction. For the coefficients of density gradient terms we use their empirical values of $D_{pp} = D_{nn} = D_{np} = 132$ MeV $\cdot$ fm^5 consistent with the Skyrme-Hartree-Fock calculations [28,33]. At $k_{min} = [(\frac{4\pi e^2}{\beta})^{1/2} - k_{TF}^2]^{1/2}$, the $V_{dyn}(k)$ has the minimal value of $V_{dyn}(k_{min}) = V_0 + 2(4\pi e^2 \beta)^{1/2} - \beta k_{TF}^2$ [2–5,28]. Its vanishing point determines the ρ_t.

The thermodynamical method requires the system to obey the intrinsic stability condition [34] or the following inequalities [7,30]

$$-\left(\frac{\partial P}{\partial v}\right)_\mu > 0, \tag{2}$$

$$-\left(\frac{\partial \mu}{\partial q_c}\right)_v > 0. \tag{3}$$

These conditions are equivalent to require the convexity of the energy per particle in the single phase [7,30] by ignoring the finite size effects due to surface and Coulomb energies as shown in the following. In the above, the $P = P_b + P_e$ is the total pressure of the *npe* system with the contributions P_b and P_e from baryons and electrons, respectively. The v and q_c are the volume and charge per baryon number. The μ is the chemical potential defined as

$$\mu = \mu_n - \mu_p. \tag{4}$$

In fact, Eq. (2) is simply the well-known mechanical stability condition of the system at a fixed μ. It ensures that any local density fluctuation will not diverge. On the other hand, Eq. (3) is the charge or chemical stability condition of the system at a fixed density. It means that any local charge variation violating the charge neutrality condition will not diverge. If the β-equilibrium condition is satisfied, namely, $\mu = \mu_e$, the electron contribution to the pressure P_e is only a function of the chemical potential μ, and in this case one can rewrite Eq. (2) as

$$-\left(\frac{\partial P_b}{\partial v}\right)_\mu > 0. \tag{5}$$

By using the relation $\frac{\partial E(\rho, x_p)}{\partial x_p} = -\mu$, one can get [30]

$$-\left(\frac{\partial P}{\partial v}\right)_\mu = 2\rho^3 \frac{\partial E(\rho, x_p)}{\partial \rho} + \rho^4 \frac{\partial^2 E(\rho, x_p)}{\partial \rho^2}$$

$$- \rho^4 \left(\frac{\partial^2 E(\rho, x_p)}{\partial \rho \partial x_p}\right)^2 \Big/ \frac{\partial^2 E(\rho, x_p)}{\partial x_p^2} > 0 \tag{6}$$

$$-\left(\frac{\partial q_c}{\partial \mu}\right)_v = 1 \Big/ \frac{\partial^2 E(\rho, x_p)}{\partial x_p^2} + \frac{\partial \rho_e}{\partial \mu_e} \Big/ \rho, \tag{7}$$

where $q_c = x_p - \rho_e / \rho$. $\rho = 1/v$ is the baryon density and $E(\rho, x_p)$ is the energy per baryon for the nucleonic matter. Within the free Fermi gas model, the density of electrons ρ_e is uniquely determined by the electron chemical potential μ_e. Then the thermodynamical relations Eqs. (2) and (3) are identical to [7,30]

$$-\left(\frac{\partial P_b}{\partial v}\right)_\mu = \rho^2 \left[2\rho \frac{\partial E(\rho, x_p)}{\partial \rho} + \rho^2 \frac{\partial^2 E(\rho, x_p)}{\partial \rho^2}\right.$$

$$\left. - \left(\frac{\partial^2 E(\rho, x_p)}{\partial \rho \partial x_p}\rho\right)^2 \Big/ \frac{\partial^2 E(\rho, x_p)}{\partial x_p^2}\right] > 0, \tag{8}$$

$$-\left(\frac{\partial q_c}{\partial \mu}\right)_v = 1 \Big/ \frac{\partial^2 E(\rho, x_p)}{\partial x_p^2} + \frac{\mu_e^2}{\pi^2 \hbar^3 \rho} > 0, \tag{9}$$

respectively. The second inequality is usually valid. Thus, the following condition from the first one,

$$V_{ther} = 2\rho \frac{\partial E(\rho, x_p)}{\partial \rho} + \rho^2 \frac{\partial^2 E(\rho, x_p)}{\partial \rho^2}$$

$$- \left(\frac{\partial^2 E(\rho, x_p)}{\partial \rho \partial x_p}\rho\right)^2 \Big/ \frac{\partial^2 E(\rho, x_p)}{\partial x_p^2} > 0, \tag{10}$$

determines the thermodynamical instability region.

Based on general thermodynamic relations and $\frac{\partial \mu_n}{\partial \rho_p} = \frac{\partial \mu_p}{\partial \rho_n}$, one can show [33]

$$\frac{2}{\rho} \frac{\partial E}{\partial \rho} \frac{\partial^2 E}{\partial x_p^2} + \frac{\partial^2 E}{\partial \rho^2} \frac{\partial^2 E}{\partial x_p^2} - \left(\frac{\partial^2 E}{\partial \rho \partial x_p}\right)^2$$

$$= \frac{\partial \mu_n}{\partial \rho_n} \frac{\partial \mu_p}{\partial \rho_p} - \left(\frac{\partial \mu_n}{\partial \rho_p}\right)^2. \tag{11}$$

Thus, for $\partial^2 E/\partial x_p^2 > 0$, Eq. (10) is equivalent to requiring a positive bulk term V_0 in Eq. (1). Generally speaking, ρ_t is in the subsaturation density region where $\partial^2 E/\partial x_p^2$ is almost always positive for all models. Therefore, the thermodynamical stability condition is simply the limit of the dynamical one as $k \to 0$ by neglecting the Coulomb interaction.

To locate the inner edge of the neutron star crust, we use the same MDI (Momentum Dependent Interaction) EOS that was used in analyzing the isospin diffusion in heavy-ion reactions [16,17]. The MDI interaction is based on a modified finite-range Gogny effective interaction [35] and has been extensively used in our previous work [14]. The baryon potential energy density part of the MDI EOS can be expressed as [16,35,36]

$$V(\rho, T, \delta) = \frac{A_u \rho_n \rho_p}{\rho_0} + \frac{A_l}{2\rho_0}(\rho_n^2 + \rho_p^2)$$

$$+ \frac{B}{\sigma + 1} \frac{\rho^{\sigma+1}}{\rho_0^\sigma}(1 - x\delta^2) + \frac{1}{\rho_0} \sum_{\tau, \tau'} C_{\tau, \tau'}$$

$$\times \iint d^3 p d^3 p' \frac{f_\tau(\vec{r}, \vec{p}) f_{\tau'}(\vec{r}, \vec{p}')}{1 + (\vec{p} - \vec{p}')^2 / \Lambda^2}. \tag{12}$$
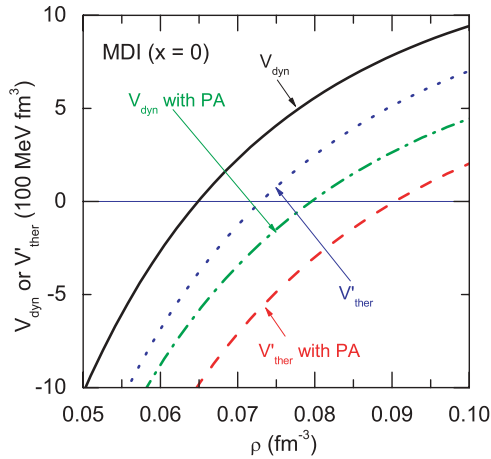
FIG. 1. (Color online) The density dependence of V_{dyn} and V'_{ther} for MDI interaction with $x = 0$ using both the dynamical and the thermodynamical methods with the full EOS and its parabolic approximation (PA).

FIG. 2. (Color online) The ρ_t as a function of L from the dynamical and thermodynamical methods with and without the parabolic approximation in the MDI interaction. The triangles are obtained by Kubis [30] and the star with an error bar represents $L = 86 \pm 25$ MeV.

Here τ is $1/2$ $(-1/2)$ for neutrons (protons) and $\delta = 1 - 2x_p$ is the isospin asymmetry. The meaning and values of other parameters can be found in Refs. [16] and [35]. The parameter x is introduced to vary only the density dependence of the symmetry energy while keeping other properties of the nuclear EOS fixed [16]. In particular, the symmetry energy $E_{sym}(\rho) = \frac{1}{2}(\frac{\partial^2 E}{\partial \delta^2})_{\delta=0}$ at saturation density $\rho_0 = 0.16$ fm^{-3} is fixed at 30.54 MeV for all values of the parameter x. The isospin symmetric part of the MDI EOS was shown to agree with the experimental constraints obtained from relativistic heavy-ion collisions up to about five times the saturation density [37].

III. RESULTS

First, to show how the uniform *npe* matter becomes stable from unstable with increasing baryon density and how to locate the transition density and see the difference between the dynamical and thermodynamical methods as well as effects of the PA, we show in Fig. 1 the density dependence of V_{dyn} and V'_{ther} using the MDI interaction with $x = 0$ within both the dynamical and thermodynamical methods with the full EOS and its PA. Here, we have defined

$$V'_{ther} = V_{ther} \frac{\partial^2 E}{\partial x_p^2} \bigg/ \left(\rho^2 \frac{\partial \mu_n}{\partial \rho_n} \right) \qquad (13)$$

and it should be noted that V'_{ther} has the same vanishing point as the V_{ther} and the same dimension as the V_{dyn}. For the MDI interaction with $x = 0$ the transition densities using the full EOS within the dynamical and the thermodynamical method are 0.065 fm^{-3} and 0.073 fm^{-3}, respectively. While the corresponding results using the PA are 0.080 and 0.090 fm^{-3}, respectively. Thus, the transition densities are generally lower with the dynamical method as the density gradient term and the Coulomb interaction make the system more stable. However, the PA significantly lifts the transition density regardless of the approach used. In fact, the difference between calculations
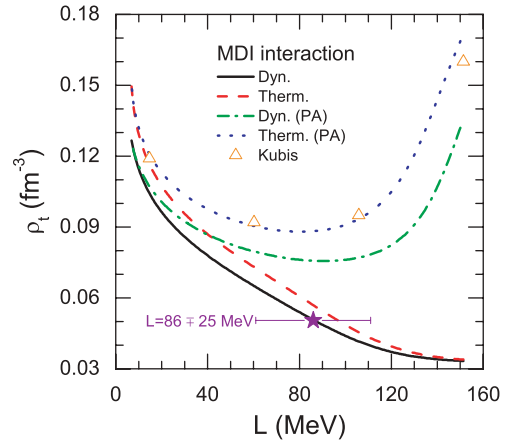
using the full EOS and its PA is much larger than that caused by using the two different methods.

Shown in Fig. 2 is the ρ_t as a function of the slope parameter of the symmetry energy $L = 3\rho_0 \frac{\partial E_{sym}(\rho)}{\partial \rho} |_{\rho=\rho_0}$ with the MDI interaction. For comparisons, we have included results using both the dynamical and the thermodynamical methods with the full EOS and its parabolic approximation, i.e., $E(\rho, \delta) = E(\rho, \delta = 0) + E_{sym}(\rho)\delta^2 + O(\delta^4)$ from the same MDI interaction. With the full MDI EOS, it is clearly seen that the ρ_t decreases almost linearly with increasing L for both methods. This feature is consistent with the RPA results [32]. It is interesting to see that both the dynamical and the thermodynamical methods give very similar results with the former giving slightly smaller ρ_t than the later (the difference is actually less than 0.01 fm^{-3}) and this is due to the fact that the former includes the density gradient and Coulomb terms that make the system more stable and lower the transition density. The small difference between the two methods implies that the effects of density gradient terms and the Coulomb term are unimportant in determining the ρ_t. On the other hand, surprisingly, the PA drastically changes the results, especially for stiffer symmetry energies (larger L values). Also included in Fig. 2 are the predictions by Kubis using the PA of the MDI EOS in the thermodynamical approach [30]. Furthermore, we find that in the parabolic approximation, using the EOS of $E(\rho, \delta) = E(\rho, \delta = 0) + [E(\rho, \delta = 1) - E(\rho, \delta = 0)]\delta^2 + O(\delta^4)$ leads to almost the same results. The large error introduced by the PA is understandable because the β-stable *npe* matter is usually highly neutron rich and the contribution from the higher order terms in δ is appreciable. This is especially the case for the stiffer symmetry energy that generally leads to a more neutron-rich *npe* matter at subsaturation densities. In addition, simply because of the energy curvatures involved in the stability conditions, the contributions from higher order terms in the EOS are multiplied by a factor larger than the quadratic term. These features agree with the early finding [38]

that the ρ_t is very sensitive to the fine details of the nuclear EOS. We notice that the EOS of asymmetric nuclear matter always contains the higher order terms in isospin asymmetry (at least for the kinetic part of the EOS). Our results indicate that one may introduce a huge error by assuming *a priori* that the EOS is parabolic for a given interaction in calculating the ρ_t. We thus apply the experimentally constrained L to the ρ_t-L correlation obtained using the full EOS in constraining the ρ_t. In the following, we mainly focus on the dynamical method because it is more complete and realistic.

The transport model analysis of the isospin diffusion data from heavy-ion collisions allowed us to constrain the parameter x in Eq. (12) to be between $x = 0$ and $x = -1$ in the density range of $0.3\rho_0$ and $1.2\rho_0$ [16,17]. With the full MDI EOS, the slope parameter was determined to be $L = 86 \pm 25$ MeV. The approximately 30% error in L is systematic in nature mainly because of the uncertainty of the in-medium nucleon-nucleon cross sections used in the transport model [17]. The statistical errors in both the data analysis [15] and the model calculations [16,17] are less than the systematic error. The error in L will lead to roughly similar systematic errors in all quantities we study here. As shown in Fig. 2, the constrained L then limits the transition density to 0.040 fm$^{-3} \leqslant \rho_t \leqslant 0.065$ fm^{-3}. It is interesting to mention that both approaches used here for finding the core-crust transition density in the *npe* matter in neutron stars have also been widely used in studying the spinodal decomposition density associated with the liquid-gas phase transition in nuclear matter, see, e.g., Refs. [39–42] for some recent applications in neutron-rich matter. As expected, see, e.g., Ref. [43], the two phase transitions are asymptotically but inherently related. Applying both the dynamical and thermodynamical approaches to symmetric nuclear matter (SNM) at zero temperature for MDI interaction by ignoring the Coulomb and surface terms, we find a transition density of $0.63\rho_0$. It is consistent with the spinodal decomposition density for SNM at zero temperature from the relativistic mean field model [39] and Skyrme density functionals [41]. On the other hand, recent studies [44,45] indicate that some effects beyond the mean field approximation may affect the EOS of asymmetric nuclear matter in the low-density region. Thus, it would be interesting to study how the effects beyond the mean field approximation as well as other effects such as the many-body forces may change the core-crust transition density of neutron stars.

The pressure at the inner edge, P_t, is also an important quantity that might be measurable indirectly from observations of pulsar glitches [7,9]. Shown in Fig. 3 is the P_t as functions of L and ρ_t by using the dynamical method with both the full MDI EOS and its PA. Again, it is seen that the PA leads to huge errors for larger (smaller) L (ρ_t) values. For the full MDI EOS, the P_t decreases (increases) with the increasing L (ρ_t) while it displays a complex relation with L or ρ_t for the PA. The complex behaviors are due to the fact that the ρ_t does not vary monotonically with L for the PA as shown in Fig. 2. From the constrained L values, the P_t is limited between 0.01 and 0.26 MeV/fm^3.

The constrained values of ρ_t and P_t have important implications for many properties of neutron stars [4,7,10,28].
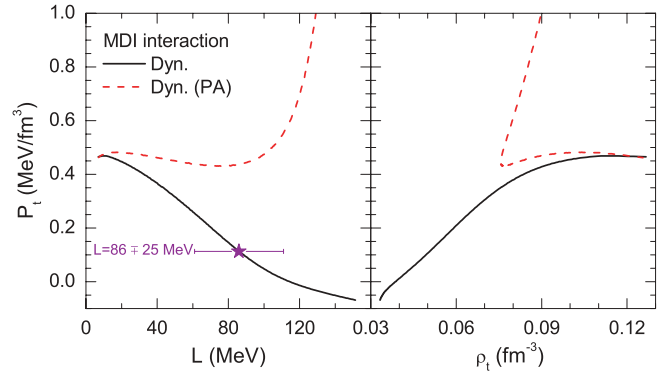

FIG. 3. (Color online) The P_t as functions of L and ρ_t by using the dynamical method with and without parabolic approximation in the MDI interaction. The star with an error bar in the left panel represents $L = 86 \pm 25$ MeV.

As an example, here we examine their impact on constraining the mass-radius (M-R) correlation of neutron stars. The crustal fraction of the total moment of inertia $\Delta I / I$ can be well approximated by [6,7,9]

$$\frac{\Delta I}{I} \approx \frac{28\pi P_t R^3}{3Mc^2} \frac{(1 - 1.67\xi - 0.6\xi^2)}{\xi}$$
$$\times \left[1 + \frac{2P_t(1 + 5\xi - 14\xi^2)}{\rho_t m_b c^2 \xi^2}\right]^{-1}, \qquad (14)$$

where m_b is the mass of baryons and $\xi = GM/Rc^2$ with G being the gravitational constant. As it was stressed in Ref. [6], the $\Delta I / I$ depends sensitively on the symmetry energy at subsaturation densities through the P_t and ρ_t, but there is no explicit dependence upon the higher density EOS. So far, the only known limit of $\Delta I / I > 0.014$ was extracted from studying the glitches of the Vela pulsar [9]. This together with the upper bounds on the P_t and ρ_t ($\rho_t = 0.065$ fm^{-3} and $P_t = 0.26$ MeV/fm^3) sets approximately a minimum radius of $R \geqslant 4.7 + 4.0M/M_\odot$ km for the Vela pulsar. The radius of the Vela pulsar is predicted to exceed 10.5 km should it have a mass of $1.4M_\odot$. A more restrictive constraint will be obtained from the lower bounds of $\rho_t = 0.040$ fm^{-3} ($P_t = 0.01$ MeV/fm^3), which is indicated by the curve with solid stars in Fig. 4, and it can be approximately parametrized by $R = 5.5 + 14.5M/M_\odot$ km. It is thus seen that the error of the transition density and pressure obtained in the present work is still large and it leads to large uncertainties for the mass-radius relation of the Vela pulsar. As a conservative estimate, we thus deduce a constraint of $R \geqslant 4.7 + 4.0M/M_\odot$ km using the upper bounds on the P_t and ρ_t obtained in the present work. We notice that a constraint of $R \geqslant 3.6 + 3.9M/M_\odot$ km for this pulsar has previously been derived in Ref. [9] by using $\rho_t = 0.075$ fm^{-3} and $P_t = 0.65$ MeV/fm^3. However, the constraint obtained in the present work using for the first time data from both the terrestrial laboratory experiments and astrophysical observations is significantly different and actually it is more stringent.

To put the above constraints on the Vela pulsar in perspective, we show them in Fig. 4 together with the M-R relation by solving the Tolman-Oppenheimer-Volkoff (TOV) equation. In
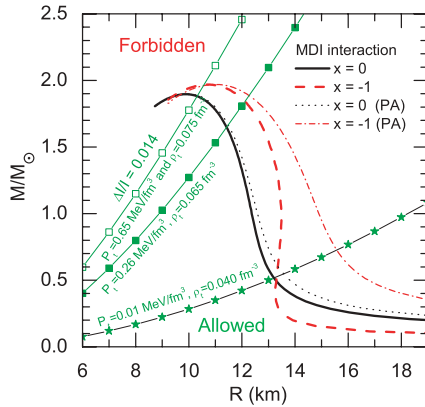
FIG. 4. (Color online) The M-R relation of static neutron stars from the full EOS and its parabolic approximation in the MDI interaction with $x = 0$ and $x = -1$. For the Vela pulsar, the constraint of $\Delta I/I > 0.014$ implies that allowed masses and radii lie to the right of the line linked with solid squares ($\rho_t = 0.065$ fm^{-3} and $P_t = 0.26$ MeV/fm^3, the upper bounds obtained in the present work), solid stars ($\rho_t = 0.040$ fm^{-3} and $P_t = 0.01$ MeV/fm^3, the lower bounds obtained in the present work), or open squares ($\rho_t = 0.075$ fm^{-3} and $P_t = 0.65$ MeV/fm^3, used in Ref. [9]).

the latter, we use the well-known BPS EOS [2] for the outer crust. In the inner crust with $\rho_{out} < \rho < \rho_t$, the EOS is largely uncertain and, following Ref. [27], we use an EOS of the form $P = a + b\epsilon^{4/3}$ with the constants a and b determined by the total pressure P and the total energy density ϵ at ρ_{out} and ρ_t. The full MDI EOS and its parabolic approximation with $x = 0$ and $x = -1$ are used for the uniform liquid core with $\rho \geqslant \rho_t$. In this way, the P is a continuous function of the ϵ at the boundary between different regions as required. Assuming that the core consists of only the npe matter without possible new degrees of freedom or phase transitions at high densities, the PA leads to a larger radius for a fixed mass compared to the full MDI EOS. Furthermore, using the full MDI EOS with $x = 0$ and $x = -1$ constrained by the heavy-ion reaction experiments, the radius of a canonical neutron star of $1.4M_\odot$ is tightly constrained

within 11.9 to 13.2 km, which is consistent with the constraint $R \geqslant 4.7 + 4.0 M/M_\odot$ km for the Vela pulsar.

IV. SUMMARY

In summary, the density and pressure at the inner edge separating the liquid core from the solid crust of neutron stars are determined to be 0.040 fm$^{-3} \leqslant \rho_t \leqslant$ 0.065 fm^{-3} and 0.01 MeV/fm$^3 \leqslant P_t \leqslant$ 0.26 MeV/fm^3, respectively, using the MDI EOS of neutron-rich nuclear matter constrained by the recent isospin diffusion data from heavy-ion reactions in the same subsaturation density range as the neutron star crust. These constraints allow us to set a new limit on the radius of the Vela pulsar. It is significantly different from the previous estimate and thus puts a new constraint for the mass-radius relation of neutron stars. Furthermore, we find that the widely used parabolic approximation to the EOS of asymmetric nuclear matter leads systematically to significantly higher core-crust transition densities and pressures, especially for the energy density functional with stiffer symmetry energies. Our results thus indicate that one may introduce a huge error by assuming *a priori* that the EOS is parabolic with respect to isospin asymmetry for a given interaction in locating the inner edge of neutron star crusts.

[1] J. M. Lattimer and M. Prakash, Science **304**, 536 (2004).
[2] G. Baym, C. Pethick, and P. Sutherland, Astrophys. J. **170**, 299 (1971).
[3] G. Baym, H. A. Bethe, and C. J. Pethick, Nucl. Phys. **A175**, 225 (1971).
[4] C. J. Pethick and D. G. Ravenhall, Annu. Rev. Nucl. Part. Sci. **45**, 429 (1995).
[5] C. J. Pethick, D. G. Ravenhall, and C. P. Lorenz, Nucl. Phys. **A584**, 675 (1995).
[6] J. M. Lattimer and M. Prakash, Phys. Rep. **333**, 121 (2000); Astrophys. J. **550**, 426 (2001).
[7] J. M. Lattimer and M. Prakash, Phys. Rep. **442**, 109 (2007).
[8] A. W. Steiner, M. Prakash, J. M. Lattimer, and P. J. Ellis, Phys. Rep. **410**, 325 (2005).
[9] B. Link, R. I. Epstein, and J. M. Lattimer, Phys. Rev. Lett. **83**, 3362 (1999).
[10] C. J. Horowitz, M. A. Perez-Garcia, and J. Piekarewicz, Phys. Rev. C **69**, 045804 (2004); C. J. Horowitz, M. A. Perez-Garcia,

J. Carriere, D. K. Berry, and J. Piekarewicz, *ibid.* **70**, 065806 (2004).
[11] A. Burrows, S. Reddy, and T. A. Thompson, Nucl. Phys. **A777**, 356 (2006).
[12] B. J. Owen, Phys. Rev. Lett. **95**, 211101 (2005).
[13] S. B. Ruster, M. Hempel, and J. Schaffner-Bielich, Phys. Rev. C **73**, 035804 (2006).
[14] B. A. Li, L. W. Chen, and C. M. Ko, Phys. Rep. **464**, 113 (2008).
[15] M. B. Tsang *et al.*, Phys. Rev. Lett. **92**, 062701 (2004).
[16] L. W. Chen, C. M. Ko, and B. A. Li, Phys. Rev. Lett. **94**, 032701 (2005).
[17] B. A. Li and L. W. Chen, Phys. Rev. C **72**, 064611 (2005).
[18] D. Shetty, S. J. Yennello, and G. A. Souliotis, Phys. Rev. C **75**, 034602 (2007).
[19] T. Li *et al.*, Phys. Rev. Lett. **99**, 162503 (2007).
[20] A. W. Steiner and B. A. Li, Phys. Rev. C **72**, 041601(R) (2005).

[21] L. W. Chen, C. M. Ko, and B. A. Li, Phys. Rev. C **72**, 064309 (2005).

[22] D. G. Ravenhall, C. J. Pethick, and J. R. Wilson, Phys. Rev. Lett. **50**, 2066 (1983).

[23] K. Oyamatsu, Nucl. Phys. **A561**, 431 (1993).

[24] A. W. Steiner, Phys. Rev. C **77**, 035805 (2008).

[25] F. Douchin and P. Haensel, Phys. Lett. **B485**, 107 (2000).

[26] F. Douchin and P. Haensel, Astron. Astrophys. **380**, 151 (2001).

[27] J. Carriere, C. J. Horowitz, and J. Piekarewicz, Astrophys. J. **593**, 463 (2003).

[28] K. Oyamatsu and K. Iida, Phys. Rev. C **75**, 015801 (2007).

[29] C. Ducoin, Ph. Chomaz, and F. Gulminelli, Nucl. Phys. **A789**, 403 (2007).

[30] S. Kubis, Phys. Rev. C **76**, 025801 (2007); **70**, 065804 (2004).

[31] A. Worley, P. G. Krastev, and B. A. Li, Astrophys. J. **685**, 390 (2008).

[32] C. J. Horowitz and J. Piekarewicz, Phys. Rev. Lett. **86**, 5647 (2001); Phys. Rev. C **64**, 062802(R) (2001); **66**, 055803 (2002).

[33] J. Xu, L. W. Chen, B. A. Li, and H. R. Ma, arXiv:0901.2309v1.

[34] H. B. Callen, *Thermodynamics and An Introduction to Thermostatistics,* 2nd edition (John Wiley & Sons, New York, 1985).

[35] C. B. Das, S. Das Gupta, C. Gale, and B. A. Li, Phys. Rev. C **67**, 034611 (2003).

[36] L. W. Chen, C. M. Ko, and B. A. Li, Phys. Rev. C **76**, 054316 (2007).

[37] P. G. Krastev, B. A. Li, and A. Worley, Phys. Lett. **B668**, 1 (2008).

[38] J. Arponen, Nucl. Phys. **A191**, 257 (1972).

[39] H. Müller and B. D. Serot, Phys. Rev. C **52**, 2072 (1995).

[40] B. A. Li and C. M. Ko, Nucl. Phys. **A618**, 498 (1997).

[41] J. Margueron and P. Chomaz, Phys. Rev. C **67**, 041602(R) (2003).

[42] J. Xu, L. W. Chen, B. A. Li, and H. R. Ma, Phys. Rev. C **77**, 014302 (2008).

[43] P. J. Siemens, Nature (London) **305**, 410 (1983).

[44] J. Margueron, E. van Dalen, and C. Fuchs, Phys. Rev. C **76**, 034309 (2007).

[45] A. Rios, A. Polls, A. Ramos, and H. Müther, Phys. Rev. C **78**, 044314 (2008).